Materials Science-Poland, 36(4), 2018, pp. 597-608
http://www.materialsscience.pwr.wroc.pl/
DOI: 10.2478/msp-2018-0082

Synthesis, growth, structural, thermal and third order nonlinear optical properties of novel organic single crystal: 4-methylpyridinium 3-nitrophthalate

S. Reena Devi[1], S. Suresh[1], S.Kalaiyarasi[1], M. NizamMohideen[2], R. Mohan Kumar[1,*]

[1]Department of Physics, Presidency College, Chennai-600 005, India
[2]Department of Physics, The New College (Autonomous), Chennai-600 014, India

A novel 4-methylpyridinium 3-nitrophthalate (4MP3NP) was synthesized and the crystals were grown by using slow evaporation method. The structural data of the grown crystal was collected by single crystal X-ray diffraction. It revealed that the 4MP3NP crystal belongs to triclinic crystal system with a space group $P\bar{1}$. Structure of the synthesized compound was established using SHELXL 97 program package. The crystalline nature and composition of the grown crystal was established using high resolution X-ray diffraction and FT-IR analyses. UV-Vis transmittance and photoluminescence studies revealed the optical transmission window and electronic transition mechanism of ions, respectively. The laser damage threshold of the grown crystal was estimated by Nd:YAG laser and these results were mutually related to specific heat capacity of the grown crystal. The third-order nonlinear optical susceptibility of the grown crystal was studied by Z-scan technique.

Keywords: *crystal structure; growth from solution; thermal studies; laser damage threshold studies; nonlinear optical materials*

1. Introduction

Crystallization of nonlinear optical materials is a source of second and third harmonic generation which is the fundamental basis to understand the new physical phenomena and also to realize the technological applications such as optical switching, frequency conservation, terahertz generation and detection. Much progress has been made in the conversion process for harmonic generation and transparency in visible and ultraviolet regions for device applications. The progress in NLO materials is fascinating due to their outstanding properties, such as wide transparency, processing of optical information, high laser damage threshold, etc. [1]. Organic crystals possess better nonlinear optical properties than inorganic materials, in particular, for second and third harmonic generation. In this background, organic molecules are the researchers inspiration, due to their conjugative path of delocalized π-electron system which helps to induce a path for large hyperpolarizability and appropriate orientation of the molecules. Hence, the organic molecules with large hyperpolarizability offer attractive advantages such as high speed data processing, optical information processing, electro-optic switches and optical bistability [2–5].

Pyridine and its derivatives act as guiding agents which leads to the synthesis of novel crystalline salts with interesting properties. 4-methylpyridine is a centrosymmetric aromatic compound and handling of a chiral pyridine crystal is more difficult, because of only dipole-dipole and van der Waals interactions between the molecules, but no hydrogen bonds [6]. To overcome this problem, pyridine compounds are intercalated with organic or inorganic acids and the pyridine molecule is converted into pyridinium cations with hydrogen-bonds. These molecules are held together by van der Waals interactions, therefore, the amines, ions and acids easily interact [7]. Normally, organic compounds are made up of conjugated path connected with a donor and acceptor group on its both ends, which

*E-mail: mohan66@hotmail.com

is the backbone to obtain third order nonlinear susceptibility, widely used in the area of photo- and electrochemical applications [8]. Hence, in the recent trends, the search for novel materials with large hyperpolarizabilities, high melting temperature and elongation of π-conjugated system has been observed [9]. The scope of present work includes the growth, structural properties, optical transmission, thermal and third order nonlinear optical properties, laser damage threshold and specific heat properties of the new organic 4-methylpyridinium 3-nitrophthalate (4MP3NP) single crystal.

2. Material synthesis, solubility and crystal growth

4-methylpyridine (Merck; 99 % purity) and 3-nitrophthalic acid (Spectrochem; 99.8 % purity) were used as starting materials for the synthesis of 4-methylpyridinium 3-nitrophthalate compound. The calculated amounts of starting materials were taken in equimolar ratio and dissolved in water solvent. To attain homogeneous mixing, the solution was continuously stirred for about 5 h and the precipitate of 4MP3NP crystalline substance was obtained at 35 °C using a constant temperature bath. The reaction scheme of 4MP3NP is shown in Fig. 1.

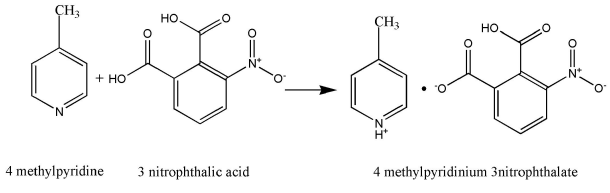

Fig. 1. Reaction scheme for synthesis of 4MP3NP.

The solubility of 4MP3NP in water was estimated from 35 °C to 50 °C using a constant temperature bath with an interval of 5 °C. A finely grinded title material was added accordingly into water and the solution was stirred continuously to reach homogeneous mixed solution. The solution was kept at a constant temperature of the bath fixed at 35 °C with an accuracy ±0.01 °C. 10 mL saturated solution was pipetted out and poured in a Petri dish. It was dried in an open atmosphere and weighed.

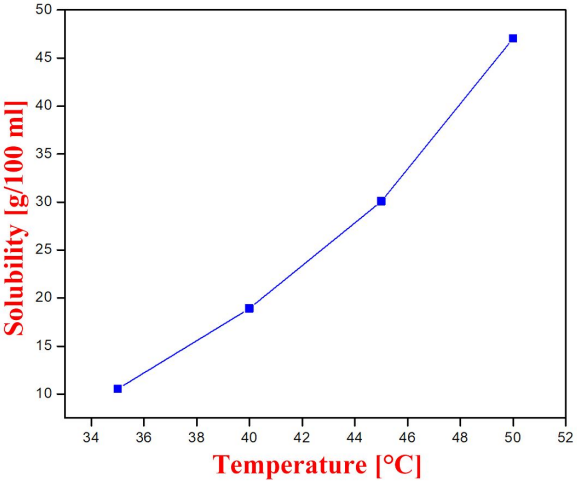

Fig. 2. Solubility curve of 4MP3NP in water solvent.

The same process was followed for different temperatures and the solubility curve of 4MP3NP was drawn as shown in Fig. 2. From this curve, it is noticed that the concentration of 4MP3NP solute increases with increasing temperature in deionized water and consequently, the title compound has positive temperature coefficient of solubility. The purification of starting materials is needed to grow transparent crystals by low temperature solution growth method. Hence, the synthesized compound was subjected to further recrystallization process and proper filtration. The saturated homogeneous solution was allowed for solvent evaporation and the supersaturated solution yielded good quality 4MP3NP crystals in a period of four weeks with dimension up to 17 mm × 14 mm × 7 mm. The photograph of the grown crystal is shown Fig. 3.

3. Results and discussion

3.1. X-ray diffraction studies

The crystal structure was determined from single-crystal X-ray diffraction data. The intensity data was collected on a Bruker Kappa APEXII single crystal X-ray diffractometer with graphite monochromated MoKα radiation ($\lambda = 0.71073$ Å)

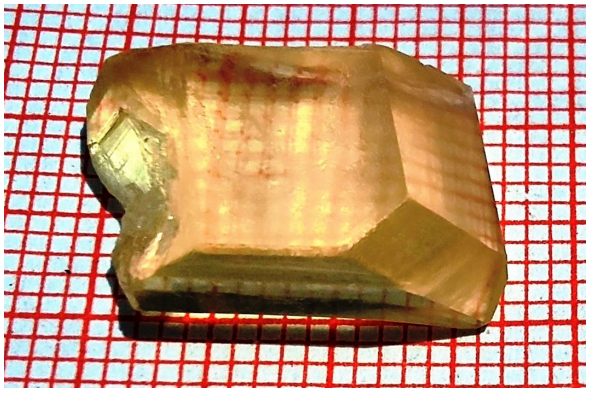

Fig. 3. Photograph of as-grown crystal of 4MP3NP.

at 293 K [10]. The structure was solved by the direct method and refined by the full matrix least-squares technique on F^2 employing the SHELXL 97 program package [11]. The asymmetric unit of the title compound comprises of two crystallographically independent 4-methylpyridinium cations and two crystallographically independent 3-nitrophthalate anions (Fig. 4).

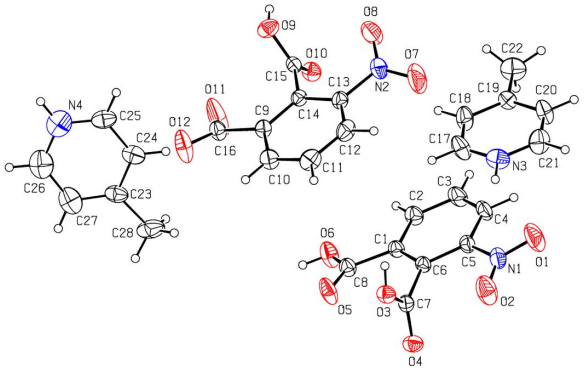

Fig. 4. ORTEP diagram of 4MP3NP crystal.

In this crystal, the cations and anions are linked via N–H...O, O–H...O and C–H...O hydrogen bonds, forming a two-dimensional network (Fig. 5).

The 4MP3NP crystallizes in triclinic crystal system with a space group $P\bar{1}$ which is centrosymmetric. The estimated cell parameters are a = 9.5078(3) Å, b = 10.7451(4) Å, c = 12.8685(5) Å, α = 70.5°(2) β = 85.8°(2) γ = 85.4°(2) and volume V = 1233.78(8) Å^3.

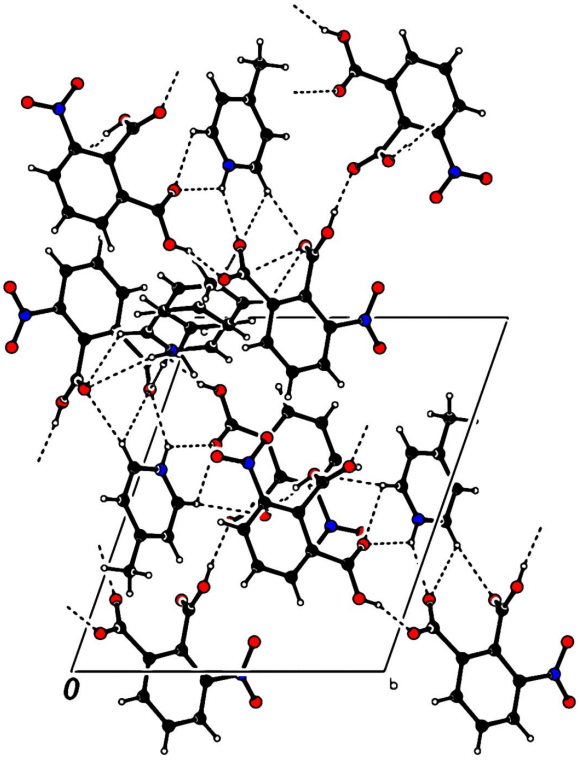

Fig. 5. Crystal packing diagram of 4MP3NP viewed along a axis.

The crystallographic data of the title compound are listed in Table 1.

The structure of 4MP3NP crystal was studied at the Cambridge Crystallographic Data Centre (CCDC# 1455686). Fig. 4 and Fig. 5 show the ORTEP diagram and crystal packing of 4MP3NP crystal, respectively. The normal probability plot analysis [12] for both bond lengths and angle shows that the difference between the two symmetry-independent molecules is of statistical nature. All the bond lengths [13] and angles are within normal ranges and they are comparable with those in closely related structures [14]. A proton transfer from the carboxyl group of the acid to the atoms N4 and N3 of 4-methyl pyridine resulted in the formation of a salt. This protonation led to widening of C25N4C26 and C17N3C21 with the angles of the pyridine rings of 119.3°(2) and 120.9°(2), compared to 115.3°(2) in the unprotonated pyridine. This type of protonation has been observed in various pyridine acid complexes [15].

Table 1. Crystal data and structure refinement for 4MP3NP.

Identification code	4MP3NP
Empirical formula	$C_{25}H_{20.50}N_{3.50}O_{12}$
Formula weight	561.95 [g/mol]
Temperature	293(2) [K]
Wavelength	0.71073 [Å]
Crystal system	Triclinic
Space group	$P\bar{1}$
Unit cell dimensions	a = 9.5078(3) Å α = 70.503(2)° b = 10.7451(4) Å β = 85.784(2)° c = 12.8685(5) Å γ = 85.406(2)°
Volume	1233.78(8) [Å^3]
Z	2
Density (calculated)	1.513 [g/cm^3]
Absorption coefficient	0.123 [mm^{-1}]
F(000)	582
Crystal size	0.300 mm × 0.200 mm × 0.200 mm
Theta range for data collection	2.152° to 24.994°.
Index ranges	$-11 \leqslant h \leqslant 11$, $-12 \leqslant k \leqslant 12$, $-15 \leqslant l \leqslant 15$
Reflections collected	21978
Independent reflections	4341 [R(int) = 0.0287]
Completeness to θ = 24.994°	99.9 %
Absorption correction	Semi-empirical from equivalents
Max. and min. transmission	0.91 and 0.89
Refinement method	Full-matrix least-squares on F2
Data/restraints/parameters	4341/119/403
Goodness-of-fit on F2	1.025
Final R indices [I>2 σ(I)]	R1 = 0.0486, wR2 = 0.1178
R indices (all data)	R1 = 0.0778, wR2 = 0.1460
Extinction coefficient	n/a
Largest diff. peak and hole	0.452 and –0.449 [e·Å^{-3}]
CCDC No.	1455686

The examination of pyridinium rings shows that these units are planar with a mean deviation of 0.001(2) and 0.001(2) Å for atoms C21 and C24, from the mean planes defined by the six constituent atoms. The dihedral angle between the 4-methylpyridinium cation and 3-nitrophthalate anion are 13.2°(2) and 72.6°(2) for the both molecules, respectively. In both molecules, the protonated 4-methylpyridinium cation is essentially planar, with maximum deviations of 0.008(2) for atom C20 and 0.012(2) Å for atom C25. The entire 4-methylpyridinium cation (C23-C28/N4) is disordered, which is confirmed by the large displacement parameters for C and N atoms and short C–C and C–N bond lengths. The disorder over two positions is modeled and the geometry is standardized by soft restraints. In the title crystal, the cations and anions are linked via N–H…O, O–H…O and C–H…O hydrogen bonds, forming a two-dimensional network. The hydrogen bond geometry is shown in Table 2.

Symmetry transformations was used to generate equivalent atoms:

#1 – x + 2, –y + 1, –z + 1 #2 x,y + 1,z – 1 #3 x + 1,y,z #4 2 – x,1 – y,1 – z #5 2 – x, –y,2 – z #6 x,y,1 + z

Table 2. Hydrogen bonds for 4MP3NP [Å and °].

D-H... A	d(D-H)	d(H... A)	d(D... A)	<(DHA)
C(17)-H(17)... O(3)#1	0.93	2.42	3.235(4)	145.8
C(17)-H(17)... O(5)#	0.93	2.37	2.941(4)	119.3
C(21)-H(21)... O(10)#2	0.93	2.35	3.271(4)	171.5
C(21)-H(21)... O(11)#2	0.93	2.58	3.029(4)	110.5
C(25)-H(25)... O(10)#3	0.93	2.57	3.218(6)	126.9
C(17)-H(17) ... O(3)#1	0.93	2.42	3.235(4)	145.8
C(17)-H(17)... O(5)#1	0.93	2.37	2.941(4)	119.3
C(21)-H(21)... O(10)#2	0.93	2.35	3.271(4)	171.5
C(21)-H(21)... O(11)#2	0.93	2.58	3.029(4)	110.5
C(25)-H(25)... O(10)#3	0.93	2.57	3.218(6)	126.9
N(3) –H(3A)... O(11)#2	0.93	2.05	2.792(3)	135(4)
N(3) –H(3A)... O(5)#4	0.93	2.28	2.893(4)	123(4)
O(3) –H(3B)... O(3)#4	0.82	1.66	2.462(3)	165
N(4) –H(4A)... O(11)#3	0.86	2.28	3.121(13)	165
O(6) –H(6)... O(12)#5	0.82	1.68	2.465(3)	159
O(9) –H(9)... O(4)#6	0.82	1.73	2.548(3)	173

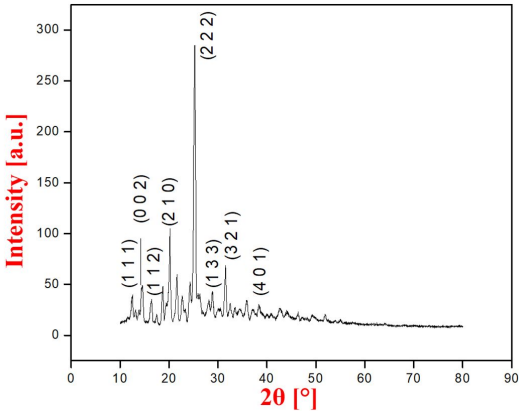

Fig. 6. Powder XRD pattern of 4MP3NP crystal.

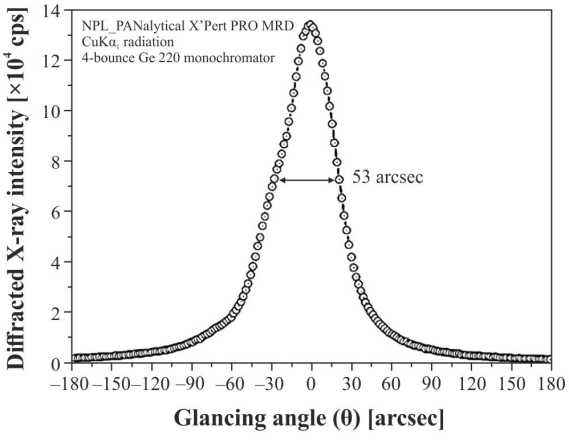

Fig. 7. HR-XRD diffraction curve of 4MP3NP crystal.

Powder X-ray diffraction pattern of the grown 4MP3NP crystal was recorded in 2θ range of 10° to 80° by employing Bruker diffractometer with CuKα radiation (Fig. 6). The prominent Bragg peaks have been indexed at specific points within 2θ range which confirmed the crystalline nature of the title compound.

The crystalline perfection of the grown crystal was examined by using HR-XRD method.

Fig. 7 shows the high resolution diffraction curve recorded for 4MP3NP single crystal using a multicrystal X-ray diffractometer with MoKα_1 radiation. As shown in Fig. 7, the DC contains a single peak without any splittings which shows that this material is free from structural grain boundaries. However, FWHM of recorded curve (53 arc sec) is much higher than the value expected by the plane wave theory of dynamical X-ray diffraction [16].

From the peak position, it shows that the particular angular deviation of glancing angle and the scattered intensity are much more shifted in the negative direction. This single broadened rocking curve with absence of any other satellite splits is ascribed to the defects such as dislocations, Schottky defects, and vacancy defects. It clearly indicates

that the crystal contains vacancy type of defects. However, these defects may be due to the presence of impurity atoms included in the solvent atoms or molecules of crystalline material. The point defects are unavoidable to some extent due to the thermal and growth condition. If the concentration is high, the FWHM would be much higher and the point defects with lesser density often lead to structural grain boundaries. Even in quantitative analysis, unavoidable defects are important in the case of phase matching applications [17]. In this investigation, the single diffraction peak with low FWHM indicates that the crystalline perfection is fairly good.

3.2. FT-IR spectral studies

Infrared spectroscopy is a useful tool for identification of the structure of molecules like coordinated compounds, providing information on the bending nature and confirmation of the material properties [18].

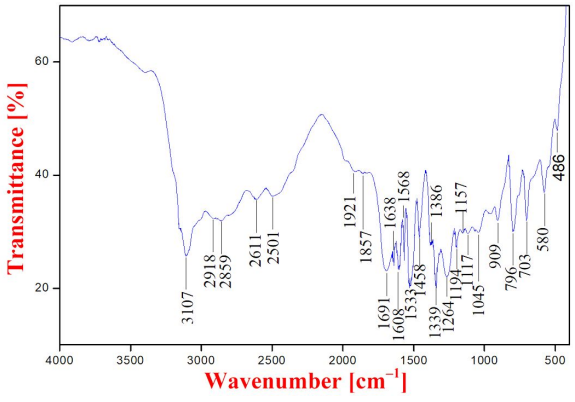

Fig. 8. FT-IR spectrum of 4MP3NP crystal.

The infrared spectrum of 4MP3NP crystal was recorded in the range 4000 cm^{-1} to 400 cm^{-1} using KBr pellet technique (Fig. 8). Aromatic ring O–H stretching vibrations occurred at 3107 cm^{-1}. The peaks occurring at 2918 cm^{-1} and 2859 cm^{-1} are due to CH_3 asymmetric and symmetric stretching. The C=N stretching vibration occurred at 1533 cm^{-1}. Frequencies appearing at 1638 cm^{-1} and 1568 cm^{-1} correspond to asymmetric and symmetric stretching vibrations, of COO^- group, respectively. The asymmetric and symmetric stretching vibrations of nitro group are found at 1458 cm^{-1} and 1339 cm^{-1}. The C–O stretching vibration appeared as a strong band around 1264 cm^{-1}. The FT-IR spectral assignments of the functional groups of the title compound are presented in Table 3.

3.3. UV-Vis-NIR studies

The optical properties of 4MP3NP crystal have been studied using UV-Vis spectrometer in the wavelength range of 200 nm to 800 nm.

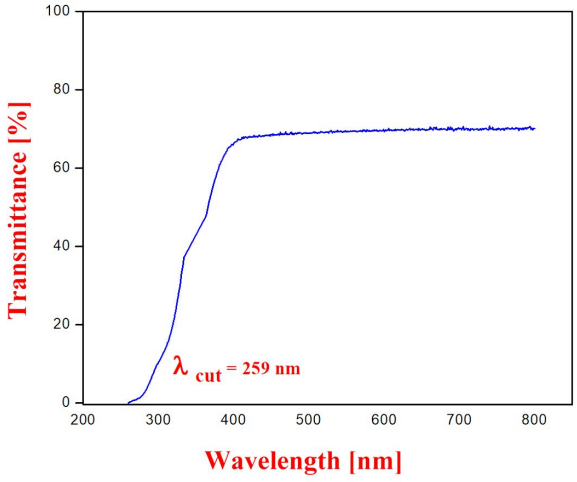

Fig. 9. UV-Vis transmittance spectrum of 4MP3NP crystal.

UV-Vis spectral analysis provides important information about different types of electronic transitions from n $\rightarrow \pi^*$ to $\sigma \rightarrow \sigma^*$. The optically polished 4MP3NP crystal was employed for recording the spectrum. The crystal was active in the entire visible region having good transparency of about 70 % and cut-off wavelength around 259 nm as shown in Fig. 9.

The optical absorption coefficient with photon energy has been used to determine the refractive index and optical band gap energy of the crystal. The absorption coefficient α, reflectance R and the refractive index n can be derived from the following relations:

$$\alpha = \frac{2.3026}{t} \log(1/T) \qquad (1)$$

Table 3. FT-IR vibrational assignments of 4MP3NP.

Wave number [cm^{-1}]	Assignment
3107	Aromatic O–H stretching
2918	CH_3 asymmetric stretching
2859	CH_3 group of ring symmetric stretching
2501	C–H symmetric stretching
1921	C=C stretching
1691	C=O stretching vibration
1608	Aromatic C=C absorption stretching
1638	COO^- asymmetric stretching
1568	COO^- symmetric stretching
1533	C=N stretching vibration
1458	Asymmetric stretching of nitro group
1339	Symmetric stretching of nitro group
1386	COO^- weak symmetrical stretching mode
1264	C–O stretching vibrations
1194	C–H bending
1157	C–H Wagging
1117	Phenolic C–O stretching vibration
1045	Aromatic ring C–H in-plane bending
796	C–H out-of-plane bending
580	COOH wagging

$$R = 1 \pm \frac{\sqrt{1-\exp(-\alpha t)+\exp(\alpha t)}}{1-\exp(-\alpha t)} \quad (2)$$

$$n = \frac{-R+1 \pm \sqrt{-3R^2+10R-3}}{2(R-1)} \quad (3)$$

where T is the transmittance and t is the thickness of crystal. The optical band gap E_g can be calculated using the relation [19]:

$$(\alpha h\nu)^2 = A(h\nu - E_g) \quad (4)$$

Fig. 10 shows the variation of $(\alpha h\nu)^2$ with $h\nu$ [20–22] in the fundamental absorption region. The band gap of the crystal was calculated from linear part of the Tauc plot and it was found to be 4.7 eV.

Theoretically, the band gap energy was calculated by using the relation:

$$E = \frac{hc}{\lambda} = \frac{6.626 \times 10^{-34} \times 3 \times 10^8}{259 \times 10^{-9} \times 1.6 \times 10^{-19}} = 4.7eV \quad (5)$$

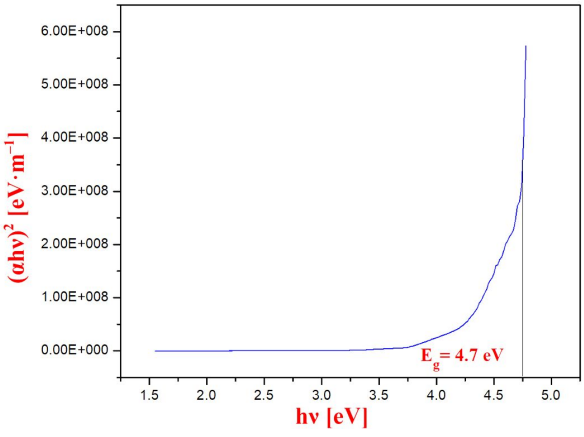

Fig. 10. Plot of $(\alpha h\nu)^2$ vs. $h\nu$ of 4MP3NP crystal.

where h is the Planck constant, c is the velocity of light and λ is the cut-off wavelength. The calculated value was verified with Tauc plot. The optical transmission range and transparency cut-off are important for NLO applications, since the title compound may be useful for fabrication of NLO devices.

3.4. Photoluminescence spectral studies

Photoluminescence analysis is a simple, versatile and nondestructive method of investigating electronic structure of materials. PL spectrum is used to ascertain the energy distribution and density of states. It is an important tool for optical process in recombination state, i.e. when light with energy greater than the band gap energy is incident on a material, which leads to the creation of electron-hole pairs in the excited states. At the excitation stage, the relaxation of electrons may occur and these electrons return to the ground state with the emission of photon energy. Due to the defect free excitation, the recombination of photon energy induces high energy phonons [23]. The PL spectrum was recorded for 4MP3NP crystal excited at 250 nm (Fig. 11).

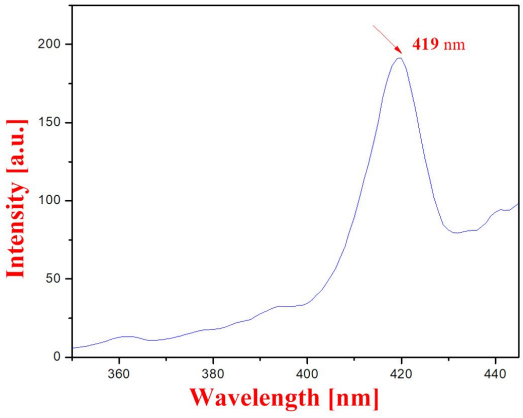

Fig. 11. Photoluminescence spectrum of 4MP3NP crystal.

A strong emission peak is observed at 419 nm. It covers the blue region of the visible spectrum which may be attributed to $\pi^* \rightarrow$ n transition. The blue emission of 4MP3NP suggests that the title material can be used in blue light emitting applications such as blue LEDs and optoelectronic devices.

3.5. Laser damage threshold studies

Laser damage threshold (LDT) of the crystal is an important factor and it can be used to analyze the withstand capacity of optical material by finding a laser damage spot caused by application of induced laser radiation. The material shows the damage due to strain and exhibits various inclusions like melting, breaking, flawing and amputating, etc. The LDT measurement was made on the plane surface of highly polished material. Hence, it produced minimum surface damage and increased the surface damage threshold. The crystal sample was mounted on an X-Y translator and the output intensity of laser, was controlled with a variable attenuator, which was delivered to the crystal surface. The energy density E of the laser beam at which the crystal gets damaged was measured.

The surface laser damage threshold of 4MP3NP crystal was calculated using the relation:

$$P_{(d)} = \frac{E}{A\tau} \tag{6}$$

where E is the intensity of the irradiation laser beam [mJ], τ is the pulse width [ns] and A is the area of the circular spot size [cm^2]. The calculated laser damage threshold value of 4MP3NP crystal is GW/cm^2. Hence, this study suggests that the 4MP3NP crystal is able to withstand a high power laser beam up to laser damage tolerance level of 4.27 GW/cm^2 which is higher than that of 4-methylpyridinium 4-hydroxybenzoate single crystal (2.79 GW/cm^2) and urea (1.5 GW/cm^2).

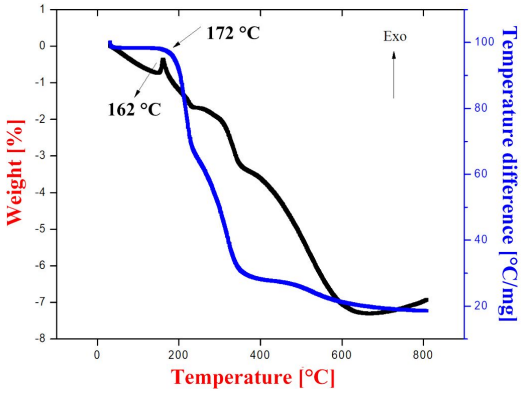

Fig. 12. TG-DTA curve of 4MP3NP crystal.

3.6. Thermal studies

Thermogravimetric and differential thermal analysis (TGA-DTA) was used to study the decomposition of the compound at a heating rate

of 10 °C/min using NETZSCH STA 449F3 instrument. Thermal stability and melting point of 4MP3NP powder sample were determined.

The resulting TGA-DTA curve of 4MP3NP is shown in Fig. 12. In the TGA curve, decomposition occurred at three different stages, when the material was heated from room temperature to 172 °C. As seen from the figure, no major weight loss occurred before 172 °C, which clearly evidences that the material is stable up to 172 °C. It reveals that there is no water molecule present in the compound. The first stage of the weight loss started at 172 °C and continued up to 236.6 °C. In the corresponding DTA curve, the sharp endothermic peak observed at 162 °C confirms the melting point of the crystal. The second weight loss continued up to 344.5 °C and it indicates that the material decomposes by emitting gaseous products, i.e. CO, CO_2, NO_2 and also hydrocarbons and amino groups. The final stage of decomposition occurred between 344.5 °C and 800 °C, where the final loss of weight of the compound was taking place. The complete decomposition occurred at the final temperature [24]. Based on the results, it can be stated that the 4MP3NP crystal is stable up to 162 °C which is useful for NLO applications.

3.7. Specific heat measurement

Specific heat measurement of 4MP3NP crystal was carried out by DSC studies in the temperature range from 30 °C to 95 °C at a heating rate of 3.5 °C/min. Fig. 13 shows the variation of specific heat capacity as a function of temperature. It is observed that the specific heat capacity increases with increasing temperature.

The specific heat of solids is one of the parameters to determine the laser damage threshold of crystal, i.e. threshold intensity (I) is directly proportional to square root of specific heat (C) of the material [25, 26]:

$$I = \frac{\sigma(1-\nu)}{S\varepsilon E} \cdot \frac{\sqrt{\pi KC\rho}}{2(1-R)\sqrt{\tau_p}} \tag{7}$$

where K is the thermal conductivity, ρ is the density, R is the reflectivity and τ_p is the pulse

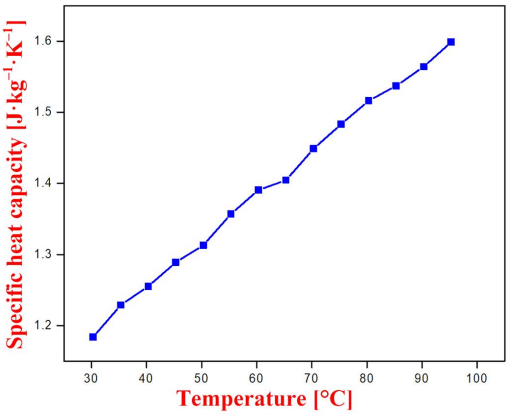

Fig. 13. Plot of specific heat capacity vs. temperature of 4MP3NP crystal.

duration. The change of thermal energy occurring in the crystal is associated with the temperature variation:

$$\Delta E = C_v \Delta T \tag{8}$$

where C_v is the specific heat and ΔT is the temperature variation. From this relation, it is observed that the temperature gradient is inversely proportional to specific heat [27].

When laser radiation penetrates into a crystal, part of the light absorbed by the crystal is converted into heat. Hence, the temperature gradient formed on the surface of the crystal causes its thermal expansion. If the thermal expansion coefficients of the crystal are anisotropic, then thermal energy observed on the surface causes its damage [28]. The cracks occurrence on the crystal during the interaction of laser was recorded through a high resolution optical microscope with a computer. The input laser energy at which the crystal get cracks was measured. The crystal has high specific heat capacity at low temperature gradient. Hence, the laser damage threshold is high for the crystal since it has low temperature gradient. The measured specific heat capacity of the compound is compatible with laser damage threshold value of 4MP3NP crystal.

3.8. Z-scan studies

Third order nonlinear optical properties of organic materials were studied by Z-scan technique.

Z-scan technique is a standard and sensitive tool to measure the intensity dependent nonlinear optical properties for investigating both sign and magnitude of nonlinear refraction n_2 and nonlinear absorption coefficient β. This method consists in measuring the nonlinear phenomena by placing a sample with or without aperture in the far field of focus as a function of Z position with respect to the focal plane. A He–Ne laser beam of 632 nm was passed for molecular excitation. By monitoring the beam transmitted through a sample with the aperture in the open arm and closed arm, it is possible to extract the nonlinear refractive index n_2 and nonlinear absorption coefficient β.

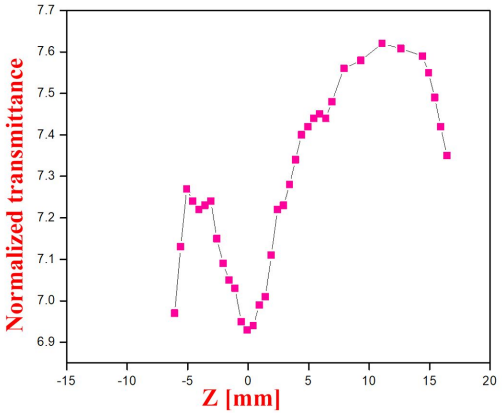

Fig. 14. Z-scan plot of 4MP3NP crystal measured in closed aperture mode.

Fig. 14 shows a characteristic closed aperture Z-scan plot of the title crystal for normalized transmittance of the incident intensity. The closed curve depicts the prefocal valley to postfocal peak arrangement which clearly suggests the nonlinear refractive index and nonlinear susceptibility of 4MP3NP crystal. Hence, a valley followed by a peak from the closed aperture Z-scan of normalized transmittance is the signature of positive refractive nonlinearity and this behavior is ascribed to self-focusing effect [29, 30]. The value of nonlinear refractive index n_2 was obtained from the difference between the normalized peak and valley transmittance ΔT_{p-v}:

$$\Delta T_{p-v} = 0.406(1-S)^{0.25}\,|\Delta\Phi o| \qquad (9)$$

where $\Delta\Phi_o$ is the on-axis phase shift at the focus, S is the linear transmittance aperture which can be calculated using the relation:

$$S = 1 - exp(-\frac{2r_a^2}{\omega_a^2}) \qquad (10)$$

where r_a is the radius of the aperture and ω_a is the diameter of the spot size in the nearest position of aperture. The nonlinear refractive index n_2 was determined by Z-scan measurement with the closed aperture:

$$n_2 = \frac{\Delta\Phi o}{kI_0L_{eff}} \qquad (11)$$

where k is the wave number ($k = 2\pi/\lambda$), I_o is the intensity of laser beam at the focus ($Z = 0$) and $L_{eff} = [1 - \exp(-\alpha L)])/\alpha$ is the effective thickness of the sample, where α is the linear absorption and L is the thickness of the sample [31].

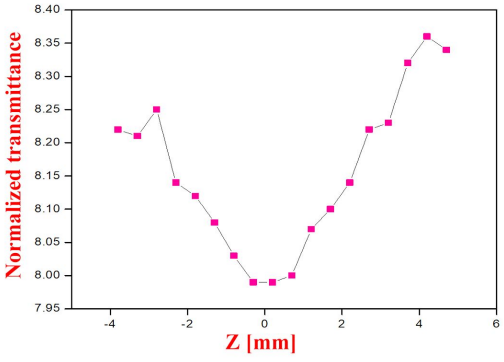

Fig. 15. Z-scan plot of 4MP3NP crystal measured in open aperture mode.

Fig. 15 shows the normalized transmission of open aperture Z-scan mode. For this measurement the aperture was removed, making the scan insensitive to nonlinear refraction.

The intensity distribution of a Gaussian laser beam could be symmetric around the focus ($Z = 0$) where it has minimum transmittance. The nonlinear absorption coefficient β was estimated by using the open aperture Z-scan data:

$$\beta = \frac{2\sqrt{2}\,\Delta T}{I_0L_{eff}} \qquad (12)$$

where $\Delta T = 1 - T_v$ is the transmittance difference between normalized condition (T = 1) and valley point at the open aperture Z-scan data [32, 33], T_v is the transmittance of the valley determined from the open aperture curve. The value of β could be positive for two photon absorption and negative for saturable absorption.

The real and imaginary part of the third order nonlinear optical susceptibility $\chi^{(3)}$ was estimated using:

$$R_e\chi^{(3)}(esu) = \frac{10^{-4}\,(\varepsilon_o C^2 n_o^2 n_2)}{\pi}(cm^2/W) \quad (13)$$

$$I_m\chi^{(3)}(esu) = \frac{10^{-2}\,(\varepsilon_o C^2 n_o^2 \lambda\beta)}{4\,\pi^2}(cm/W) \quad (14)$$

where ϵ_o is the vacuum permittivity, c is the velocity of light in vacuum, n_o is the linear refractive index of the sample and λ is the wavelength of laser beam.

The third order nonlinear optical susceptibility was calculated using the relation:

$$\chi^{(3)} = \sqrt{(R_e\chi^{(3)})^2 + (I_m\chi^{(3)})^2} \quad (15)$$

The second order hyperpolarizability has been explained by nonlinear induced polarization per molecule which is related to the third order bulk susceptibility:

$$\gamma_h = \frac{\chi^{(3)}}{L^4\,N} \quad (16)$$

where N is the density of the molecules and L is the local field factor of Lorentz approximation which is equal to:

$$L = \frac{n_0^2 + 2}{3} \quad (17)$$

where n_0 is the refractive index of the medium. From the above analysis, nonlinear refractive index and nonlinear absorption coefficient β from Z-scan data were found to be 1.409×10^{-11} cm^2/W and 2.0583×10^{-4} cm/W. By using n_2 and β values, the third order nonlinear susceptibility $\chi^{(3)} = 1.8547 \times 10^{-7}$ esu and second order hyperpolarizability ($\gamma_h = 1.126 \times 10^{-7}$ esu) were estimated and given in Table 4.

The contribution of nonlinear refractive index of 4MP3NP crystal shows that the real part of the susceptibility is relatively greater than imaginary part, correspondingly, the high value of γ_h and $\chi^{(3)}$ of the order of 10^{-6} esu are due to the presence of large and fast polarizability of a π-electron system. Hence, 4MP3NP single crystal can be utilized by various applications such as nonlinear spectroscopy, optical switching, optical logic gates and optical limiting.

4. Conclusions

Organic single crystal of 4MP3NP was grown by slow evaporation technique. X-ray diffraction study confirmed that 4MP3NP crystal belongs to triclinic system with $P\bar{1}$ space group. The crystalline perfection was studied using HR-XRD. The presence of functional groups in the grown crystal was confirmed by FT-IR spectral analysis. UV-Vis transmittance studies provided the transparency, cut-off wavelength and band gap energy of 4MP3NP crystal which confirmed importance of the material for optical devices. Photoluminescence spectral studies showed that the 4MP3NP single crystal has blue fluorescence emission, hence the material can be used in the fabrication of blue LEDs and optoelectronic devices. Laser damage threshold value of 4MP3NP (4.27 GW/cm^2) is appropriate for the fabrication of NLO devices. From TGA-DTA thermal studies, it was concluded that the grown crystal is stable up to 162 °C. The specific heat capacity study implied that the 4MP3NP crystal has high optical damage value and is suitable to operate in high temperature devices. The third order nonlinear optical parameters were estimated by Z-scan technique which confirmed the suitability of the materials to be used in third order harmonics generation. Thus, 4MP3NP seems to be a promising NLO material as the crystal possesses better optical, thermal and laser damage threshold properties compared to many well-known organic crystals.

Table 4. Third order nonlinear optical parameters of 4MP3NP crystal measured by Z-scan technique.

Parameters	Values
Nonlinear refractive index n_2	1.409×10^{-11} cm^2/W
Nonlinear absorption coefficient β	2.0583×10^{-4} cm/W
Third order nonlinear optical susceptibility $\chi^{(3)}$	1.8548×10^{-7} esu
Second order hyperpolarizability γ_h	1.126×10^{-7} esu

Acknowledgements

One of the authors (S.R) would like to acknowledge Dr. Kamalesh Kumar Mayura, National Physical Laboratory, New Delhi-110012, India, for HR-XRD studies.

References

[1] TESHOME A., BHUIYAN M.D.H., GAINSFORD G.J., ASHARF M., ASSELBERGS I., WILLIAMS G.V.M., KAY A.J, CLAYS K., *Opt. Mater.,* 33 (2011), 336.

[2] SANKAR S., MANIKANDAN M.R., RAM S.G, MAHALINGAM T., RAVI G., *J. Cryst. Growth,* 312 (2010), 2729.

[3] BABU G.A., RAMASAMY R.P., RAMASAMY P., *Mater. Chem. Phys.,* 117 (2009), 326.

[4] SHKIR M., RISCOB B., BHAGAVANNARAYANA G., *Solid State Sci.,* 14 (2012), 773.

[5] CAI Z., ZHOU M., GAO J., *Opt. Mater.,* 31 (2009), 1128.

[6] OHMS U., GUTH H., TREUTMANN W., DANNOHL H., SCHWEIG A., HEGER G., *J. Chem. Phys.,* 83 (1985), 273.

[7] MIYAZAKI T., ICHIMURA K., MATSUZAKI S., SANO M., *J. Phys. Chem. Solids*, 54 (1993), 1023.

[8] VIJAYALAKSHMI A., BALRAJ V., PERAMAIYAN G., VINITHA G., *J. Solid State Chem.,* 246 (2017), 237.

[9] SUDHAHAR S., KUMAR K.M., SORNAMURTHY B.M., KUMAR M.R., *Spectrochim. Acta A,* 118 (2014), 929.

[10] AHMAD T., ZIA-UR-REHMAN M., SIDDIQUI H., MAHMUD S., PARVVEZ M., *Acta Crystallogr. E,* 66 (2010), o976.

[11] SHELDRICK G.M., *Acta Crystallogr. A,* 64 (2008), 112.

[12] CROMER D.T., WABER J.T., *International Tables for X-ray Crystallography,* 1974, Table 2.2 A.

[13] ALLEN F.H., KENNARD O., WATSON D.G., BRAMMER L., ORPEN A.G., TAYLOR R., *J. Chem. Soc. Pakistan,* 2 (1987), S1.

[14] RAJKUMAR M.A., NIZAMMOHIDEEN M., XAVIER S.S.J., ANBARASU S., DEVARAJAN D.P.A., *Acta Crystallogr. E,* 71 (2015), 231.

[15] BABU K., SURESH S., DHAVAMURTHY M., NIZAMMOHIDEEN M., PERAMAIYAN G., MOHAN R., *Acta Crystallogr.,* 70 (2014), o600.

[16] BETTERMAN B.W., COLE H., *Rev. Mod. Phys.,* 36 (1964), 681.

[17] BHAGAVANNARAYANA G., RISCOB B., SHAKIR M., *Mater. Chem. Phys.,* 126 (2011), 20.

[18] SILVERSTEIN R.M., WEBSTER F.X., *Spectrometric identification of organic compounds,* John Wiley and Sons Publishers, New York, 2004.

[19] ZAHID I.M., KALAIYARASI S., KRISHNA KUMAR M., GANESH T., JAISANKAR V., MOHAN KUMAR R., *Mater. Sci.-Poland,* 34 (2016), 811.

[20] TAUC J., GRIGORVICI R., VANCU A., *Phys. Status Solidi B,* 15 (1966), 627.

[21] PUNIA R., KUNDU R.S., HOODA J., DHANKHAR S., SAJJAN DAHIYA., KISHORE N., *J. Appl. Phys.,* 110 (2011), 33527.

[22] URBACH F., *Phys. Rev.,* 92 (1953), 1324.

[23] KASAP S., CAPPER P., Springer *Handbook of Electronic and Photonic Materials,* Springer Science Inc., 2006, p. 47.

[24] HAMEED A.S.H., ANANDAN P., JAYAVEL R., RAMASAMY P., RAVI G., *J. Cryst. Growth,* 249 (2003), 316.

[25] BENZ R., NAOUMIDIS A., NICKEL H.,*J. Nucl. Mater.,* 150 (1987), 128

[26] VINOTHKUMAR P., KUMAR R.M., JAYAVEL R., BHASKARAN A., *Opt.Laser Technol.,* 81 (2016), 145.

[27] JAUHAR R.M., VISWANATHAN V., VIVEK P., VINITHA G., VELMURUGAN D., MURUGAKOOTHAN P., *RSC Adv.,* 6 (2016), 57977.

[28] MANIVANNAN S., DHANUSKODI S., TIWARI S.K., PHILIP J., *Appl. Phys. B-Lasers O.,* 90 (2008), 489.

[29] NANDA K., KUNDU R.S., SHARMA S., MOHAN D., PUNIA R., KISHORE N., *Solid State Sci.,* 45 (2015), 15.

[30] SHEIK-BAHAE M., SAID A.A., WEI T.H., HAGAN D.J. STRYLAND VAN E.W., *IEEE J. Quantum Elect.,* 26 (1990), 760

[31] NAGAPANDISELVI P., BABY C., GOPALAKRISHNAN R., *RSC Adv.,* 4 (2014), 22350.

[32] KARUPPASAMY P., PANDIAN M.S., RAMASAMY P., *J. Cryst. Growth,* 2017.

[33] REENA DEVI S., KALAIYARASI S., ZAHID I.M., MOHAN KUMAR R., *J. Cryst. Growth,* 454 (2016), 139.

Received 2017-03-31
Accepted 2018-07-21